International Conference on Renewable Energies and Power Quality (ICREPQ’16)
Madrid (Spain), 4th to 6th May, 2016
Renewable Energy and Power Quality Journal (RE&PQJ)
ISSN 2172-038 X, No.14 May 2016

Production of synthesis gas from dry reforming of propane with carbon dioxide over ceria-promoted nickel foam catalysts

J. Karuppiah[1], E. Linga Reddy[2], M.S.P. Sudhakaran[1] and S.B. Lee[1]

[1] Department of Chemical and Biological Engineering
Jeju National University, Jeju 690-756 (Korea)
Phone/Fax number:+82-64-754-3683/+82-64-755-3670, e-mail: sblee@jejunu.ac.kr

[2] Department of Chemical Engineering, Kyungpook
National University, Daegu 702-701 (Korea)

https://doi.org/10.24084/repqj14.443

Abstract. A series of nickel foam supported cerai catalysts (ceria/NiF) for dry reforming of propane with carbon dioxide were prepared and their performance were evaluated at temperatures in the range of 520-600°C. Among the catalysts examined the 4 wt.% CeO_2/NiF exhibited better low-temperature activity for the DRP, which is attributed to the formation of well-isolated nanosize CeO_2 particles and highly reducible metal oxide species over the NiF support. The XPS and temperature programmed reduction (TPR) data also supported the incorporation of ceria into the NiO surface layer formed over NiF support, which was substantially higher in 4% CeO_2/NF catalyst. Due to these favorable properties, the 4 wt.% CeO_2/NiF could be considered as an excellent catalyst for DRP.

Key words

Syngas, Propane reforming, Nickel foam, Ceria, Catalytic activity

1. Introduction

The generation of synthesis gas (syngas; a mixture of H_2 and CO) from hydrocarbons has received great attention owing to its wide range of applications towards sustainable and green energy technologies. Steam reforming and CO_2 dry reforming are well-known syngas production processes. The dry reforming process has widely been used to convert natural gas into syngas. Recently, catalytic dry reforming of propane (DRP) into syngas with a low H_2/CO ratio holds great promise in terms of effective utilization of CO_2 and petroleum for various small-scale applications [1-2]. Mesoporous nickel foam (NiF) with open-network structure has been considered as an excellent choice for catalysts or catalyst support for various applications [3,4]. NiF supports are ubiquitous because catalytic reactors made of NiF have many advantages over conventional packed-bed reactors, including high geometric surface area, low pressure drop even at high flow rates, efficient mass transfer, and high thermo-mechanical stability. In this work, mesoporous NiF supported ceria (CeO_2/NiF) nanocatalysts with 2, 3 and 4 wt.% nominal Ce contents have been prepared by impregnation method, which were characterized by various techniques such as X-ray diffraction (XRD), field emission scanning electron microscopy (SEM), X-ray photoelectron spectroscopy (XPS) and Raman spectroscopy.

2. Experimental

The NiF (thickness: 1.6 mm) purchased from MTI Korea was first sonicated in 10 wt.% HCl solution in order to remove surface oxide layer, and then washed with deionized water and ethanol twice. So as to incorporate CeO_2 into the NiF at different concentrations (2-4 wt.%), a simple impregnation method was used. In detail, a given amount of cerium nitrate ($Ce(NO_3)_3{\cdot}6H_2O$) was dissolved in deionized water, and the pre-treated NiF (4×4 cm^2) was immersed in the aqueous cerium nitrate solution. Finally, the NiF was taken out from the aqueous solution and dried overnight at room temperature before the calcination at 500°C for 5 h in air. The CeO_2 loading was carefully measured from the weight difference of the NiF support before and after the incorporation of CeO_2.

2.1. Catalyst activity test

The DRP with CO_2 was carried out in a thermo-catalytic reactor packed with ~4 g of the catalyst. The CeO_2/NiF catalyst prepared as above was trimmed into coin-shaped pieces (diameter: 20.8 mm) which were stacked one by one along the axis of the reactor tube. The catalytic activity was studied in the temperature range of 520-600°C for all the catalysts with different CeO_2 loadings. The reactant gases were fed into the reactor at the proportion of 10:30:60 (C_3H_8:CO_2:N_2). The total flow rate was fixed at 300 ml min^{-1} throughout this work. During the reforming reaction, the concentrations of relevant components were analyzed by the GC. The overall reaction of the DRP with CO_2 can be written as follows:

$$C_3H_8 + 3CO_2 = 6CO + 4H_2,\ \Delta H^o_{298K}=644.8\ kJmol^{-1} \qquad (1)$$

It is well known that such a strong endothermic reaction is favored at high temperatures. The conversion (X_A) of C_3H_8 or CO_2 was calculated using the equation below, taking the fractional change in the volumetric flow rate into account [5].

$$X_A(\%) = \frac{C_{A0} - C_A}{C_{A0} + \varepsilon_A C_A} \times 100(\%) \qquad (2)$$

Here, C_{A0} and C_A are the inlet and outlet concentrations of the reactant (C_3H_8 or CO_2),and ε_A is defined as

$$\varepsilon_A = \frac{\eta_{X_A=1} - \eta_{X_A=0}}{\eta_{X_A=0}} \qquad (3)$$

where $\eta_{X_A=0}$ and $\eta_{X_A=1}$ stand for the total number of moles of reactants (no conversion) and the total number of moles of products (complete conversion), respectively. For an inlet feed gas composition of C_3H_8 (10%), CO_2 (30%) and N_2 (60%), ε_A is calculated to be 0.6 by equation (3).

3. Results

Fig. 1 shows the X-ray diffractograms of the 2-4 wt. % CeO_2/NiF catalysts along with the bare NiF. In the XRD pattern, the strong diffraction peaks from NiF can be indexed to the (111), (200), and (220) planes of Ni (JCPDS 87-0712) [6]. In addition, the XRD patterns of all the three CeO_2 loaded catalysts in Fig. 1 showed well resolved cubic NiO diffraction peaks which can be indexed to the JCPDS 47-1049. Noticeably, the NiO diffraction peaks intensity has been varied corresponding to the amount of ceria loading. The absence of diffraction peak related to ceria in XRD pattern of 2 wt. % CeO_2/NiF catalyst ascribes the complete incorporation of Ce^{3+} ions into surface NiO layer. For 3 wt. % CeO_2 loaded sample, it can be seen that the formation of cubic fluorite CeO_2 phase. To our surprise the negligible intensity of NiO diffraction peaks in Fig.1c, associates the predominant phase segregation of ceria over NiF support. In the meantime, the 4 wt. % CeO_2/NiF catalyst exhibited strong diffraction peaks resulting from NiO as well as CeO_2, which may be attributed to the surface oxygen diffusion into metal support to form the more NiO layer. The diffraction peaks of CeO_2 promoted catalysts can be directly indexed to (111), (200), (220), (311), and (331) crystal faces, corresponding to the face-centered cubic-phase of CeO_2 (JCPDS 34-0394, space group Fm3m) [7-8].

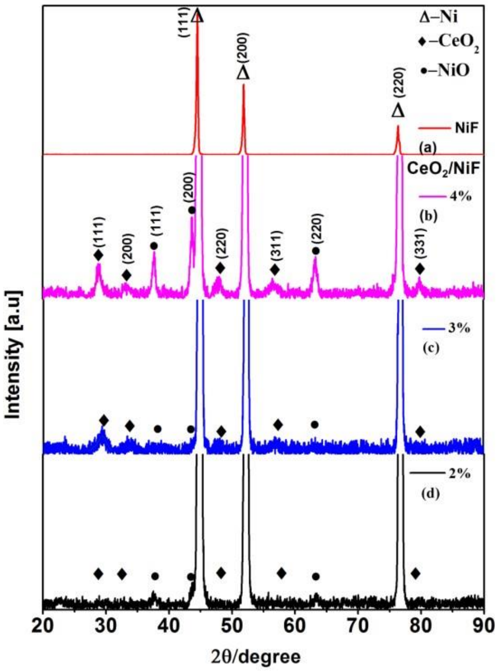

Fig. 1. X-ray diffractograms of (a) bare NiF, (b) 4 wt.% CeO$_2$/NiF, (c) 3 wt.% CeO$_2$/NiF and (d) 2 wt.% CeO$_2$/NiF.

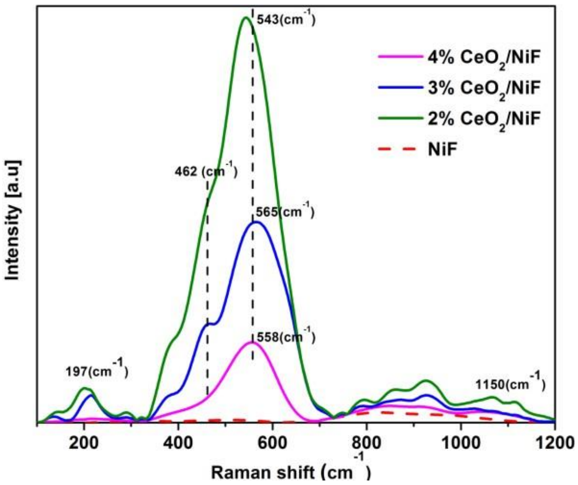

Fig. 2. Raman spectra of the NiF support and CeO$_2$/NiF catalysts with different ceria contents before the DRP.

Fig. 2 presents the Raman spectra of the 2-4% CeO$_2$ promoted NiF catalysts and bare NiF. The Raman spectrum of the bare NiF did not reflect any characteristic Raman vibrations, which indicates the metallic nature and relatively high purity of the NiF. On the other hand, the incorporation of CeO$_2$ showed significant variations in the Raman spectra. For all the catalysts, we observe Raman bands from NiO and CeO$_2$ in the spectra region of above 400 cm^{-1}. All the three spectra showed broad Raman band at 570 cm^{-1}, suggesting that the first-order one phonon (1P) LO mode of NiO layer. Whereas the low intensity Raman bands over the spectral region between 700 – 1100 cm^{-1} correspond to the second-order two phonon (2P) vibrational modes [9-11]. Noticeably, the intensity of the defect-induced D band (~570 cm^{-1}) varied with the Ce content (2-4 wt. %) according to the symmetry-breaking imperfections including defects, Ni and oxygen vacancies or disorder in the crystal lattice [12]. Furthermore, the Ni-O stretching mode has been shifted towards high frequency region from 543 cm^{-1} to 565 cm^{-1} for 2 and 3% CeO$_2$ loaded catalysts. In the case of 4% CeO$_2$ promoted catalyst, the Ni-O band ~7 cm^{-1} blue-shifted which indicates the direct influence of CeO$_2$ layer on NiO surface. The noticed peak shifts and its broadening depend on various parameters, i.e. oxygen vacancies, phonon confinement, and in homogeneous strain related to the reduced ceria [13-14]. From this observation it can be understandable that presence of defects in the CeO$_2$ promoted NiF catalysts. The ratio between defects-related band and characteristic band gives information on the relative structural disorder (RSD) in the solid solution [15]. As can be seen from **Fig. 3**, for 2 and 3 wt. % CeO$_2$/NiF catalysts show a prominent band at around 460 cm^{-1}, corresponding to the F_{2g} vibration of the cubic fluorite type CeO$_2$ that support the observations made from the XRD studies. To increase the Ce concentration to 4%, the F_{2g} band of CeO$_2$ suppressed and exhibit in negligible intensity ascribes that homogeneous dispersion of Ce ions into the NiO lattices. This is the fact that the crystallinity of the NiO improves when the CeO$_2$ layer is inserted which is concordance with the XRD results as discussed earlier. From the Raman spectra, it can be concluded that the formation of more Ce-Ni-O solid solution for the 4 wt. %CeO$_2$/NiF catalyst which leads to the excellent catalytic activity towards propane reforming reaction [16]. The additional peaks appeared at 221 and 1120 cm^{-1} may be ascribed to the stretching vibrations of Ni-O or related defects on NiF surface.

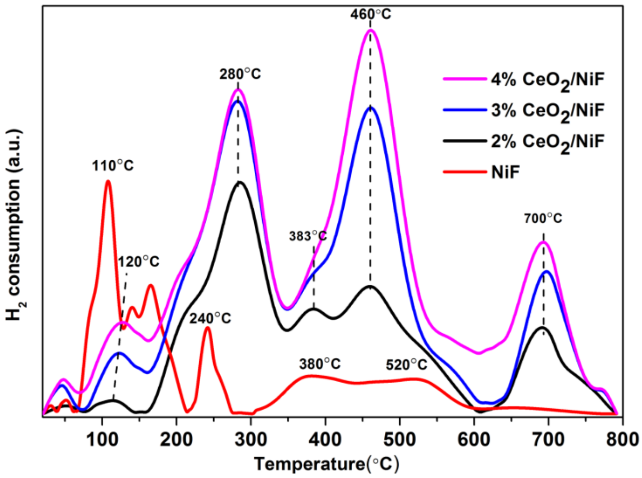

Fig. 3. TPR profiles of the NiF support and CeO$_2$/NiF catalysts with different ceria contents.

The H_2-TPR profiles of the prepared catalysts are shown in Fig. 3. It is well demonstrated that pure ceria exhibits two step reduction processes due to reduction of surface oxygen and bulk-phase lattice oxygen; one at 527°C, which is associated to the surface reduction and the other at 700 °C due to the bulk reduction. For the bare NiF, two low- temperature reduction peaks appeared at around 240°C and 380°C, and a high-temperature reduction peak at 520°C. A strong peak observed at around 110°C can be attributed to the reduction of impurities [17]. The first peak (between 300 and 450 °C) is ascribed to the reduction of the surface Ni species. The second peak (450~600 °C) is related to the reduction of bulk Ni species associated to NiF support [18-20]. However, Shan et al. explained these overlapped peaks by the different steps in the oxidation state of Ni, from Ni^{2+} to Ni^0 [21]. All the three CeO$_2$/NiF catalysts exhibited three peaks in their TPR profiles. The first peak at 280 °C resulted from the reduction of the oxygen species adsorbed on the vacant sites generated by the incorporation of Ce^{4+} ions into the NiO lattice, the second peak at 460 °C from the reduction of Ni from NiO layer, and the third peak at 700 °C from the reduction of ceria nanoparticle [22-24]. The TPR profiles of the 2 wt.% and

3 wt.%CeO_2/NiF were similar to that of the 4 wt.% equivalent. The reduction peak at around 280°C is due to lower enthalpy of reduction, the surface bounded CeO_2 are first reduced at lower temperatures followed by the reduction at around 460°C due to NiO species which has been strongly coupled with CeO_2 [22]. Besides, the intensity of the second H_2 consumption peak for the 4 wt.% CeO_2/NiF was stronger than the 2-3 wt.% equivalent, suggesting that there were more number NiO species are actively contributed to reduction reaction in combination with CeO_2.When compared to 2-3% wt%, the H_2 consumption peak area for all the three reduction process were increased significantly with the CeO_2 content, indicating that the effective contribution of ceria surface oxygen.

Fig. 4 shows the propane and CO_2 conversion efficiencies as a function of temperature. The propane and CO_2 conversion increased with increasing the temperature for all the catalysts. As the temperature increases, the oxygen mobility increases and more lattice oxygen atoms are also involved in the reaction [25], this improves the propane and CO_2 conversions. As indicated in Fig. 4, the CeO2 content had a significant influence on the catalytic performance. The bare NiF exhibited a relatively poor catalytic activity even at a temperature as high as 600°C. The conversions are gradually increased as the CeO_2 content up to 3 wt. %. Further increasing to 4 wt. % resulted in a drastic increase in the catalytic activity, even at low temperatures. The excellent conversions of propane and CO_2 were achieved with this catalyst at a temperature as low as 520°C which is about 86% and 65%, respectively, reaching 95% and 93% when the temperature reached to 600°C. Whereas, the 3 wt. %CeO_2/NiF catalyst exhibited only 63% and 57% conversions for propane and CO_2 even at 600 °C, and it is 50% and 44% for 2 wt. % CeO_2/NiF catalyst at the same temperature. Meanwhile, the CO_2 conversions obtained for the bare NiF, 2 wt.% CeO_2/NiF and 3 wt.%CeO_2/NiF over the temperature range of 520−600°C were higher than the corresponding propane conversions, which may be due to reverse water shift reaction (RWGS), but also to carbon gasification by CO_2 [26].

$$CO_2 + H_2 = H_2O + CO,\ \Delta H^o_{298K} = 41\ kJmol^{-1} \qquad 4$$

$$C + H_2O = H_2 + CO_2,\ \Delta H^o_{298K} = 131\ kJmol^{-1} \qquad 5$$

The CO_2 conversion occurs via two pathways such as the conversion of CO_2 adsorbed on CeO_2 and the dissociation of CO_2 adsorbed on oxygen vacancies. The dissociation of CO_2 adsorbed on oxygen vacancies can provide supplementary oxygen and be helpful to the oxygen mobility [27]. Among the different 2-4%CeO_2/NiF catalysts studied, the 4%CeO_2/NiF compound has been chosen not only because of its good performance in DPR activity but also because its homogeneity over NiF/NiO surface in the form of solid solution. XRD analysis of 2-4%CeO_2/NiF catalyst clearly shows NiO and CeO_2 phases that indicates the strong interaction of Ce^{4+} into NiF increases NiO phase segregation for 4% of CeO_2/NiF. These NiO species present the characteristic of being able to be reduced and reoxidized easily and generated vacancy can be refilled by CeO_2 lattice oxygen. Hence, it can be expected that the NiO species on the surface of 4%CeO_2/NiF sample provides adequate active oxygen species for DRP. The formed oxygen vacancies can be refilled by migration of the oxygen from the CeO_2 lattice due to the strong interaction between CeO_2 and Ni species (evidence from H_2-TPR studies, Raman and XRD). Therefore, it can be suggested that the reducible nature of the Ni species plays a beneficial role in the DRP activity of the 4%CeO_2/NiF.

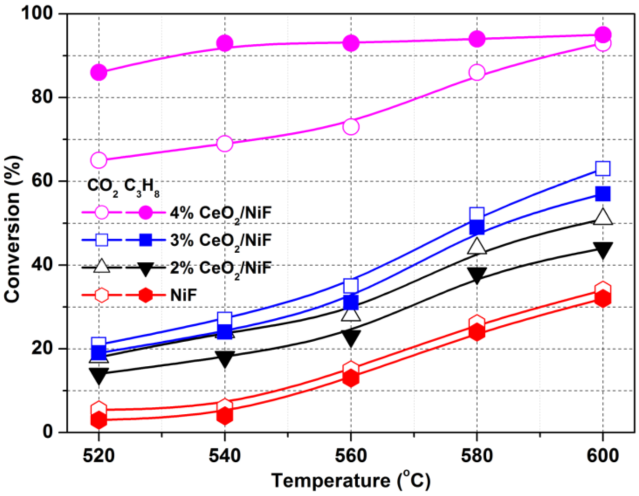

Fig. 4. C_3H_8 and CO_2 conversion efficiencies obtained with the NiF support and CeO_2/NiF catalysts with different ceria contents.

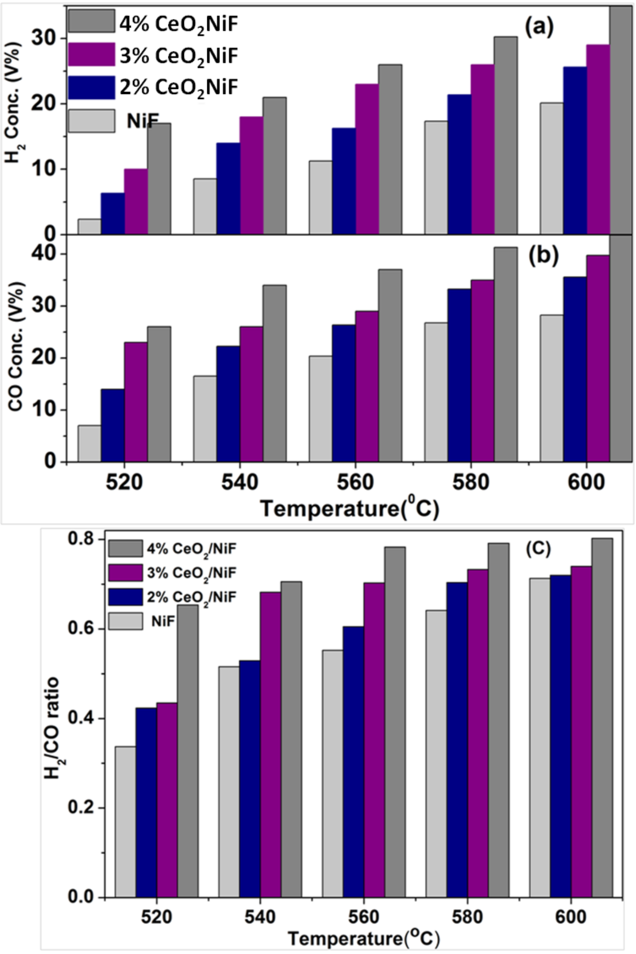

Fig. 5. Concentrations of (a) H_2 and (b) CO produced, and (c) H_2/CO ratios achieved by the NiF support and CeO_2/NiF catalysts with different ceria contents.

The concentrations of H_2 and CO during the DRP are illustrated in Fig. 5a-b. The 4 wt.% CeO_2/NiF showed higher activity than the other three catalysts in terms of H_2 and CO production. The concentration of CO was higher than that of H_2 at all temperatures, and the concentrations of both gases increased with increasing the temperature. Due to the high endothermicity of the dry reforming, an increase in the temperature is beneficial to the conversions of C_3H_8 and CO_2 and therefore the production of H_2 and

CO [28]. With 4 wt.% catalyst, the propane conversion is higher than that of CO_2 (Fig. 5), but with the other catalysts, CO_2 conversion is higher than propane conversion. However, the catalyst having the higher loading of CeO_2 exhibits higher activity. One explanation of this behavior could the high mobility of activated oxygen caused by high concentration of ceria in the lattice and surface of supports, which favors the reaction of this activated oxygen with propane from gas phase. The H_2/CO ratio obtained at various reaction temperatures is illustrated in Fig. 5c. For all the catalysts, the H_2/CO ratios were less than unity, and the ratio increased with increasing the temperature. Increasing reaction temperature led to an increased value for the ratio of H_2 /CO due to the suppressed reversed water-gas shift reaction at high temperature. At all temperatures, the H_2/CO ratio produced by the 4 wt.% CeO_2/NiF catalyst was larger than those by the other catalysts.

3.1 Long-term stability tests of CeO_2/NiF catalysts.

The long-term stability of the CeO_2/NiF catalysts for the DRP was examined at 540°C for 24 h, and the results are shown in Fig.6. As mentioned earlier in relation to Fig. 4, the incorporation of CeO_2 into the NiF enhanced the catalytic activity towards the DRP. The initial propane and CO_2 conversions obtained with the 4 wt.% CeO_2/NiF catalyst were 93 and 68 %. As shown in Fig. 6, the 4 wt.% CeO_2/NiF catalyst underwent slight deactivation after 24h, but the degree of deactivation was not significant. The propane conversion decreased to 89%, while the CO_2 conversion to 61%.The activity of the 3 wt. %, 2w% CeO_2/NiF supports was also outstandingly improved after the CeO_2 addition, which indicates the importance of CeO_2 in the dry reforming reaction for long term stability. Generally, stability of the catalysts can be reflected by three experimental phenomena: apparent thermal stability of supports and the catalysts, high metal dispersion and carbon deposition of the catalysts. Many factors including basicity of supports, concentrations of surface oxygen vacancies, oxygen storage capacity, interaction between support and metal and microstructures of the catalysts can significantly affect the observation in the morphological changes and catalytic activity of the catalysts.

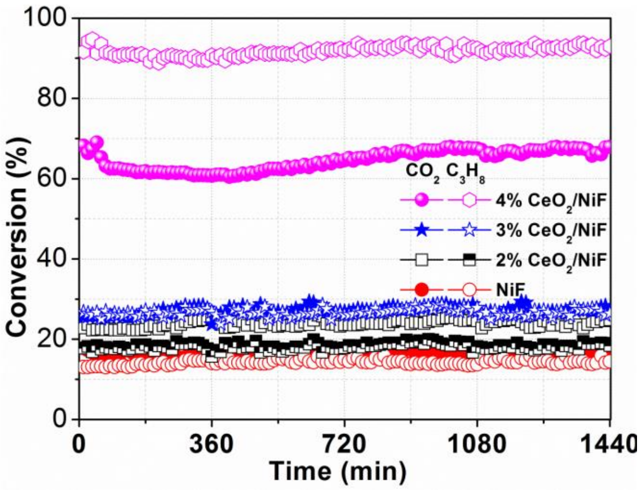

Fig. 6. Stability of the catalysts in term of CO_2&C_3H_8conversions over the time period of 24 h at 540 ºC.

It is well known that the Raman spectroscopy is the powerful tool to observe the internal chemical structure and presence of carbonaceous element. Also Raman spectra can give us the more information about the nature of carbonaceous deposits on the used catalysts. Fig. 7 displays the Raman spectra of the used catalysts, where two major peaks at 1341 cm^{-1} (D band) and 1576 cm^{-1} (G band) were clearly observed in all the used CeO_2/NiF catalysts [28]. The high intensity D-modes at 1341 cm^{-1} substantiates the presence of large amount of disordered graphitic carbon has been formed as the byproducts which reduce the catalytic activity. The ratio of intensities of the D and G maximums (I_D and I_G) gives an indication of the crystallinity of the studied material.

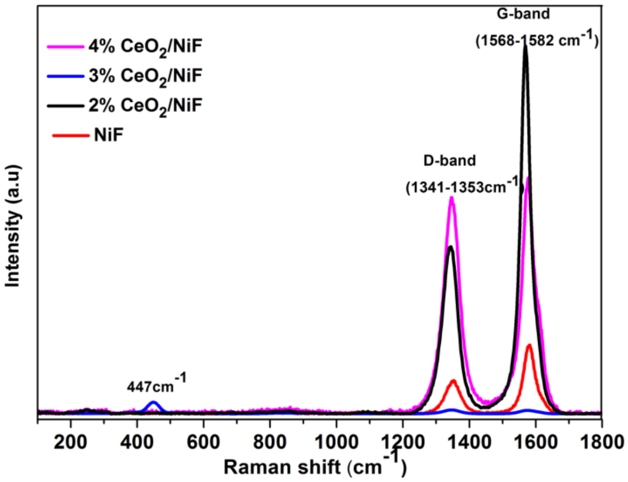

Fig. 7. Raman spectra of the catalysts after the DRP.

The lower value of I_D/I_G points out on higher crystallinity, while the higher ratio suggests on the higher disorder within the crystalline structure. Highly oriented pyrolytic graphite (HOPG) has an I_D/I_G ratio approaching 0, while amorphous carbon has a value near 3.3. The 3% CeO_2/NiF of used catalyst after reaction showed an average I_D/I_G value of ~1.3, that is, higher than the ratio (~0.91) of the 4%CeO_2/NiF catalyst indicates the more amorphous carbon was formed in 3%CeO_2 catalyst. Typical D-mode peaks for 3%CeO_2 catalyst exhibit the as equal to G-band (±10) as shown in Fig.7. However, in 4% CeO_2/NiF, 2% CeO_2/NiF, and bare NiF, D band is less intense than the G band. It seemed that carbon species were not uniformly distributed over the catalyst surface [29]. According to earlier reports band is much more intense despite a higher disorder degree. These may be explained by the different carbon species are presented with some better ordered than others [29].

4. Conclusions

In summary, 2-4 wt. %CeO_2/NiF catalysts were prepared by wet impregnation method and characterized by various techniques. The XRD results suggested the formation of nano-oxides with sizes of ~5-16 nm. The Raman band at 620 cm^{-1} indicated that the lattice oxygen was significantly higher in 4% CeO_2/NF sample. XRD analysis revealed the formation of a rich ceria phase at higher loading >3% CeO_2 on NF. TPR measurements revealed strong interactions between CeO_2 and NiF support and that facilitate reduction at lower temperatures. In addition, various sized CeO_2 nano particles with spherical morphology were dispersed over the surface of the supports. The TPR data also supported the incorporation of ceria into the NiO surface layer formed over NiF support, which was substantially higher in 4% CeO_2/NF catalyst. Due to these favorable properties, the 4 wt. % CeO_2/NiF could be considered as an excellent catalysts for propane reforming reaction. DRP with CO_2 over the prepared catalysts follows the order 4 wt. % CeO_2/NiF>3 wt.% CeO_2/NiF>2 wt.% CeO_2/NiF> bare NiF. Among the different catalysts, the 4 wt. % CeO_2/NiF catalyst showed excellent activity at 540ºC and~92% of propane and 70% of CO_2 conversion. The better DRP activity of 4 wt. % CeO_2/NiF is due to the fluorite lattice of ceria and the accompanied generation of oxygen vacancies in the catalyst. As a result, the higher catalytic activity, better catalytic stability and higher coke resistance of 2-4 wt.% CeO_2/NiF catalysts for the DRP reaction demonstrates that the novel ceria promoted porous NiF as a promising support for high temperature catalytic reaction.

Acknowledgements

This research was supported by Basic Science Research Program through the National Research Foundation of Korea (NRF) funded by the Ministry of Science, ICT and Future Planning (Grant No. 2013R1A2A2A01067961).

References

[1] A. Jha, D.-W. Jeong, W.-J. Jang, C. V. Rode and H.-S. Roh, *RSC Advances*, 2015, **5**, 1430-1437.
[2] L. B. Råberg, M. B. Jensen, U. Olsbye, C. Daniel, S. Haag, C. Mirodatos and A. O. Sjåstad, *Journal of Catalysis*, 2007, **249**, 250-260.
[3] X. Xiong, D. Ding, D. Chen, G. Waller, Y. Bu, Z. Wang and M. Liu, *Nano Energy*, 2015, **11**, 154-161.
[4] J. Xiong, X. Dong, Y. Dong, X. Hao and S. Hampshire, *International Journal of Hydrogen Energy*, 2012, **37**, 12307-12316.
[5] J. Karuppiah and Y. S. Mok, *Int. J. Hydrogen Energy*, 2014, **39**, 16329-16338.
[6] H. Yan, D. Zhang, J. Xu, Y. Lu, Y. Liu, K. Qiu, Y. Zhang and Y. Luo, Nanoscale Res Lett, 2014, 9, 1-7.
[7] J. Zhang, H. Yang, S. Wang, W. Liu, X. Liu, J. Guo and Y. Yang, Cryst.Eng. Comm, 2014, 16, 8777-8785.
[8] C. Sun, J. Sun, G. Xiao, H. Zhang, X. Qiu, H. Li and L. Chen, J. Phys. Chem. B, 2006, 110, 13445-13452.
[9] L. De Los Santos Valladares, A. Ionescu, S. Holmes, C. H. W. Barnes, A. Bustamante Domínguez, O. Avalos Quispe, J. C. González, S. Milana, M. Barbone, A. C. Ferrari, H. Ramos and Y. Majima, J. Vac. Sci. Technol B, 2014, 32, 051808.
[10] R. E. Dietz, W. F. Brinkman, A. E. Meixner and H. J. Guggenheim, Phys. Rev. Lett, 1971, 27, 814-817.
[11] R. E. Dietz, G. I. Parisot and A. E. Meixner, Phys. Rev. B: Condens. Matter, 1971, 4, 2302-2310.
[12] P. A. Fleury and R. Loudon, Phys. Rev, 1968, 166, 514-530.
[13] P. Sudarsanam, B. Mallesham, D. N. Durgasri and B. M. Reddy, RSC Advances, 2014, 4, 11322-11330.
[14] B. M. Reddy, P. Bharali, P. Saikia, A. Khan, S. Loridant, M. Muhler and W. Grünert, Phys. Chem. C, 2007, 111, 1878-1881.
[15] S. Rossignol, F. Gerard, D. Mesnard, C. Kappenstein and D. Duprez, J. Mater. Chem, 2003, 13, 3017-3020.
[16] S. Mahammadunnisa, P. Manoj Kumar Reddy, N. Lingaiah and C. Subrahmanyam, Catal. Sci. Technol, 2013, 3, 730-736.
[17] A. Zawadzki, J. D. A. Bellido, A. F. Lucrédio and E. M. Assaf, Fuel Process. Technol, 2014, 128, 432-440.
[18] J. Marrero-Jerez, A. Murugan, I. S. Metcalfe and P. Núñez, Ceram. Int, 2014, 40, 15175-15182.
[19] Y. Wei, H. Wang, K. Li, X. Zhu and Y. Du, J. Rare Earths, 2010, 28, Supplement 1, 357-361.
[20] L. Liu and L. Hong, Appl. Catal., A, 2013, 459, 89-96.
[21] W. Shan, M. Luo, P. Ying, W. Shen and C. Li, Appl. Catal., A, 2003, 246, 1-9.
[22] J. Hu, C. Yu, Y. Bi, L. Wei, J. Chen and X. Chen, Chinese J. Catal, 2014, 35, 8-20.
[23] B. Zapata, M. A. Valenzuela, J. Palacios and E. Torres-Garcia, Int. J. Hydrogen Energy, 2010, 35, 12091-12097.
[24] L. Pino, A. Vita, F. Cipitì, M. Laganà and V. Recupero, Appl. Catal., B, 2011, 104, 64-73.
[25] V. Balcaen, R. Roelant, H. Poelman, D. Poelman and G. B. Marin, Catal. Today, 2010, 157, 49-54.
[26] A. Serrano-Lotina and L. Daza, Int. J. Hydrogen Energy, 2014, 39, 4089-4094.
[27] A. Pantazidis, S. A. Bucholz, H. W. Zanthoff, Y. Schuurman and C. Mirodatos, Catal. Today, 1998, 40, 207-214.
[28] S. Zhang, S. Muratsugu, N. Ishiguro and M. Tada, ACS Catalysis, 2013, 3, 1855-1864.
[29] D. Liu, X. Y. Quek, W. N. E. Cheo, R. Lau, A. Borgna and Y. Yang, J. Catal, 2009, 266, 380-390.